Philosophical Magazine
Publication details, including instructions for authors and subscription information:
http://www.tandfonline.com/loi/tphm20

Mobile effect of hydrogen on intergranular decohesion of iron: first-principles calculations

Masatake Yamaguchi [a], Jun Kameda [b], Ken-Ichi Ebihara [a], Mitsuhiro Itakura [a] & Hideo Kaburaki [a]

[a] Center for Computational Science and e-Systems, Japan Atomic Energy Agency, Tokai-mura, Ibaraki 319-1195, Japan

[b] New Industry Creation Hatchery Center, Tohoku University, 6-6-10 Aoba, Aramaki, Aoba-ku Sendai 980-8579, Japan

Published online: 16 Jan 2012.

To cite this article: Masatake Yamaguchi, Jun Kameda, Ken-Ichi Ebihara, Mitsuhiro Itakura & Hideo Kaburaki (2012) Mobile effect of hydrogen on intergranular decohesion of iron: first-principles calculations, Philosophical Magazine, 92:11, 1349-1368, DOI: 10.1080/14786435.2011.645077

To link to this article: http://dx.doi.org/10.1080/14786435.2011.645077

Philosophical Magazine
Vol. 92, No. 11, 11 April 2012, 1349–1368

Taylor & Francis
Taylor & Francis Group

Mobile effect of hydrogen on intergranular decohesion of iron: first-principles calculations

Masatake Yamaguchi[a]*, Jun Kameda[b], Ken-Ichi Ebihara[a], Mitsuhiro Itakura[a] and Hideo Kaburaki[a]

[a]*Center for Computational Science and e-Systems, Japan Atomic Energy Agency, Tokai-mura, Ibaraki 319-1195, Japan;* [b]*New Industry Creation Hatchery Center, Tohoku University, 6-6-10 Aoba, Aramaki, Aoba-ku Sendai 980-8579, Japan*

(*Received 19 October 2011; final version received 23 November 2011*)

Atomistic mechanisms of hydrogen-induced cracking along a bcc Fe Σ3(111) symmetrical tilt grain boundary (GB) have been studied by first-principles calculations. The mobile and immobile effects of hydrogen on the GB decohesion are analyzed by calculating the dependence of hydrogen segregation energy on the coverage relevant to the repulsive interaction among segregated hydrogen atoms at the GB and on its fracture surfaces, together with generalizing McLean's formula. It was found that the segregation of combined mobile and immobile hydrogen atoms from the bulk and/or GB on the fracture surfaces causes much stronger reduction (70–80%) in the GB cohesive energy. It can occur even at a very low bulk hydrogen content of about 10^{-9} atomic fraction during slow cracking. This is in contrast to only 10–20% decohesion induced by immobile hydrogen at much higher hydrogen content during fast cracking. The mobile effect of hydrogen, giving rise to a profound reduction in the GB cohesive energy, is a key factor controlling the mechanism of hydrogen-induced GB cracking.

Keywords: first-principles calculations; intergranular decohesion; segregation; iron; mobile and immobile effect of hydrogen

1. Introduction

It is well recognized that hydrogen possesses several unique properties in iron and ferritic steels at ambient temperatures, for example, low solubility, high diffusivity, and strong interactions with many types of structural defects, such as grain boundary (GB), crack, dislocation, surface, precipitate, and vacancy [1]. Therefore, hydrogen absorbed in ferritic alloys produces remarkable influence on the deformation and fracture behavior [1–3]. Among the degradation behavior of several mechanical properties caused by hydrogen, brittle cracking along GBs and lath martensite interfaces can be readily observed in medium- and high-strength ferritic steels in gaseous and aqueous hydrogen environments. Although a number of mechanisms of hydrogen embrittlement have been presented [4–8], it is yet to be envisioned as to

*Corresponding author. Email: yamaguchi.masatake@jaea.go.jp

ISSN 1478–6435 print/ISSN 1478–6443 online

http://dx.doi.org/10.1080/14786435.2011.645077
http://www.tandfonline.com

how hydrogen promotes decohesion along grain or lath boundaries and enhances or suppresses the plasticity.

The thermodynamic theory of the mobile and immobile effects of solute on intergranular decohesion has been proposed by Rice and/or Hirth [9,10], and later elaborated by Rice and Wang [11]. The intergranular cohesive energy is differently represented depending on the conditions of constant composition and chemical potential in terms of the energy difference between the GB and its two fracture surfaces (FSs), and the interplay of the solute mobility and decohesion rate. Kameda [12] has applied the theory to demonstrate how the intergranular and crack-surface segregation of hydrogen influence the threshold stress intensity for slow and fast GB cracking, despite some drawbacks of decohesion modeling. As illustrated in Figure 1a, the immobile effect of hydrogen is identical to temper embrittlelement by segregated phosphorous (P) and sulfur (S), the quantity of which

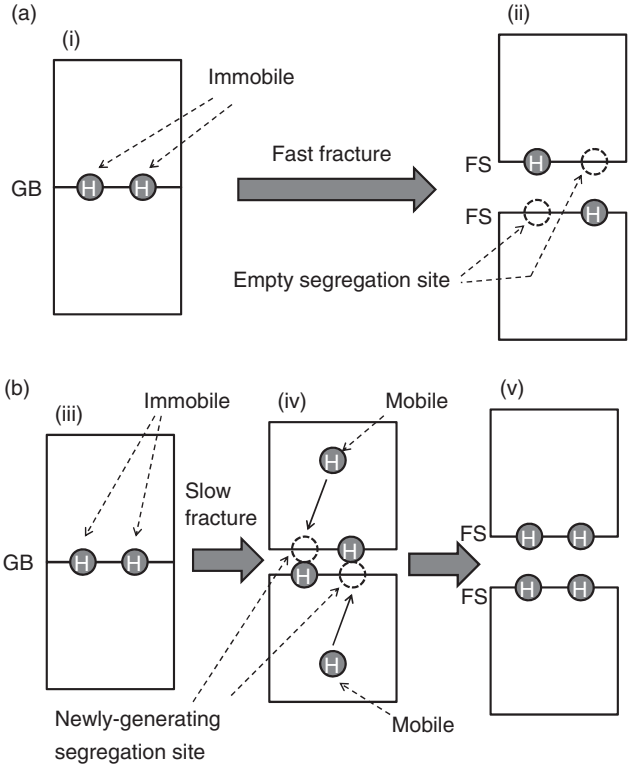

Figure 1. Schematic illustration of mobile and immobile effects of hydrogen at crack tip during crack propagation. (a) Immobile effect of hydrogen during fast crack propagation under the condition of constant composition: (i) before fracture; (ii) after fracture. (b) Mobile and immobile effects of hydrogen during slow crack propagation under the condition of constant chemical potential: (iii) before fracture; (iv) bond-stretching decohesion zone that has newly generated segregation sites; and (v) after fracture. GB: grain boundary; FS: fracture surface. Later discussion suggests that most of mobile hydrogen that segregates in the bond-stretching zone probably comes from the bulk not directly but through the GB.

remains the same along the GB and the two FSs. In this case, solute elements cannot be diffusible during brittle crack propagation and some segregation sites on the fracture surfaces remain empty after fracture, as shown in Figure 1a-ii. Therefore, it is called the condition of constant composition. When hydrogen atoms are capable of migrating from the bulk or a GB region adjacent to the crack tip and are trapped in the newly generated segregation sites (Figure 1b-iv), on the other hand, the mobile effect of hydrogen causes localized decohesion by further increasing the segregation on the two FSs. Such mobile hydrogen would promote slow cracking under the condition of constant chemical potential.

The significant advancement in computers and codes has the potential of studying the interaction energy of hydrogen atoms with lattice defects such as grain boundaries and vacancies based on first-principles calculations. A reduction in the intergranular cohesive energy ($2\gamma_{\text{int}}$) of a bcc Fe $\Sigma3(111)$ GB by hydrogen segregation has been inferred by Zhong et al. by first-principles calculations for the first time [13]. After this study, the segregation of hydrogen along the iron GB and the effect on decohesion has been further analyzed [14,15]. Nonetheless, those studies have not investigated the variation of the GB segregation energy with coverage, which arises from the repulsive interactions among densely segregated hydrogen atoms. In addition, those studies have not even mentioned the mobile effect of hydrogen.

Our more detailed first-principles studies [16,17] on the effect of various segregated solutes, such as boron (B), carbon (C), P, S, and hydrogen, on the GB decohesion in iron have been carried out by determining two kinds of solute segregation energy defined over a unit-cell area and a single segregated solute atom, respectively, as a function of the number of segregated hydrogen atoms. The former as well as the latter, designated as the derivative (incremental) one, were used for the calculation of the cohesive energy and solute segregation. It has been shown that whether solute segregation weakens or strengthens bcc Fe $\Sigma3(111)$ GB is largely controlled by the surface activity of the segregated solute. Strong surface-active solutes, such as P, S, and hydrogen cause intergranular embrittlement by reducing the surface energy on the FS much more than the GB energy, whereas segregation of weak surface-active B and C toughens the GB by mainly decreasing the GB energy more than the FS energy. Additionally, hydrogen reduces more strongly the cohesive energy of Al than those of Fe and Cu, depending on the magnitude of the surface-energy drop caused by hydrogen segregation. One of the specific implications [17] is that mobile hydrogen atoms possibly play a more significant role on intergranular slow cracking (decohesion) than immobile hydrogen, as suggested in References [9–12].

To extend our effort to quantify the hydrogen effect on the GB cohesive energy under various bulk hydrogen contents and temperatures, it is of importance to incorporate the hydrogen mobility and segregation energy along the GB and FS. The GB cracking mechanism is illustrated in Appendix A and the FS signifies the microcrack surface. In this article, the correlations of two types of hydrogen segregation energy over a unit-cell area and a single segregated hydrogen atom with hydrogen coverage have been explicitly established at the bcc Fe $\Sigma3(111)$ GB and its FS to generalize McLean's formula of equilibrium segregation [18]. This makes it possible to determine how mobile hydrogen segregation more than the immobile segregation predominantly controls GB cracking.

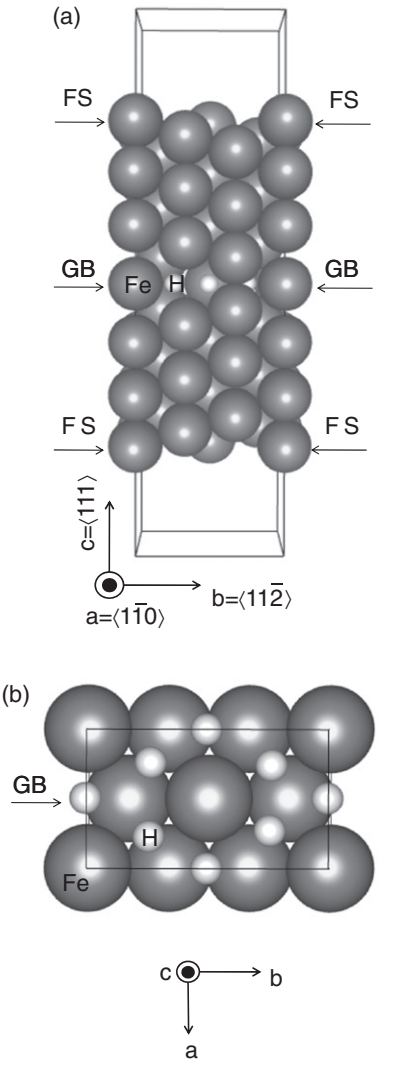

Figure 2. The unit cell including bcc Fe Σ 3(111) symmetrical tilt grain boundary (GB) and (111) fracture surfaces (FSs). The lengths of vectors **a**, **b**, and **c** of the cell are 0.401, 0.693, and 2.553 nm, respectively. The large and small spheres indicate Fe and H atoms, respectively. In this figure, the GB plane is fully covered by H atoms at the sites, which have been previously the octahedral sites in the bcc Fe lattice. (a) Side view; (b) top view of GB plane. The unit-cell area of GB/FS defined by vectors **a** and **b** is 0.278 nm^2 ($=A$). The optimized lattice constant of bcc Fe cell (2 atom/cell) is 0.2832 nm.

2. Calculations

2.1. *Modeling of grain boundary and electronic structure calculations*

For the first-principles calculations, we used a unit cell including the bcc Fe Σ3(111) symmetrical tilt GB comprising a tilt angle of 70.5 degrees and a rotation axis of ⟨1$\bar{1}$0⟩ as shown in Figure 2. A vacuum region is introduced in the upper and lower

regions of this cell to allow grain boundary sliding along the GB plane. Two surfaces denoted by FS in Figure 2 are just the same as the fracture surfaces of this GB. This cell consists of 38 iron atoms. This grain boundary has a simple structure and relatively high energy. For the calculations of GB and FS energies, we prepared a different unit cell that is almost the same as the unit cell shown in Figure 2, but which does not include the grain boundary. The unit-cell area defined by vectors **a** and **b** along the GB/FS plane is denoted by A ($= 0.278\,\mathrm{nm}^2$).

First-principles calculations were performed for ferromagnetic bcc Fe systems. The electronic structure calculation and the atomic structure relaxation by force minimization are made by using the Vienna Ab initio Simulation Package (VASP), together with the Projector Augmented Wave (PAW) method [19–21]. The generalized gradient approximation of Perdew, Burke, and Ernzerhof (PBE) [22] is applied to calculate the spin-polarized ferromagnetic state. The Methfessel–Paxton smearing method with 0.1-eV width is used. The cutoff energy and the k-point mesh are mentioned next. The zero-point energy of hydrogen and the contribution of vibrational entropy are not considered in this article, as they will be done in our future work.

2.2. *Solid-solution energy and segregation energy of hydrogen*

The grain-boundary/fracture-surface segregation energy can be defined as the energy gains of the segregation state with regard to the solid–solution state. For this reason, the solid–solution energy of hydrogen is first calculated in a bcc Fe $4 \times 4 \times 4$ super-cell (128 Fe atoms/cell). A single hydrogen atom is inserted at an interstitial octahedral (o) or tetrahedral (t) site in this super-cell, and the atomic positions and the cell are fully relaxed so as to minimize the atomic forces and cell stresses. In this calculation, we use 30% higher cutoff energy (350 eV) than a standard one for Fe (268 eV), and a $3 \times 3 \times 3$ Monkhorst–Pack k-point mesh. The solid–solution energy can be defined in terms of the total energy of the system with and without a single hydrogen atom at an interstitial o site or t site in the bcc Fe $4 \times 4 \times 4$ super-cell ($E_{\mathrm{tot}}^{\mathrm{super}}(128\mathrm{Fe}, 1\mathrm{H})$ and $E_{\mathrm{tot}}^{\mathrm{super}}(128\mathrm{Fe})$), and the total energy of the hydrogen molecule ($E_{\mathrm{tot}}(\mathrm{H}_2)$). That is

$$\Delta E_{\mathrm{sol}} = E_{\mathrm{tot}}^{\mathrm{super}}(128\mathrm{Fe}, 1\mathrm{H}) - E_{\mathrm{tot}}^{\mathrm{super}}(128\mathrm{Fe}) - \frac{1}{2}E_{\mathrm{tot}}(\mathrm{H}_2), \tag{1}$$

where $E_{\mathrm{tot}}(\mathrm{H}_2)$ is calculated using a 1 nm × 1 nm × 1 nm vacuum cell, the same cutoff energy, and only the gamma point.

The GB/FS segregation energy is calculated using the cell (38 Fe atom/cell), as shown in Figure 2. The segregation energy of the number (n) of hydrogen atoms is defined in Equation (2),

$$\Delta E_{\mathrm{gb/s}}^{\mathrm{seg}}(n) = E_{\mathrm{tot,gb/s}}^{\mathrm{GB}}(38\mathrm{Fe}, n\mathrm{H}) - E_{\mathrm{tot}}^{\mathrm{GB}}(38\mathrm{Fe}) - \frac{n}{2}E_{\mathrm{tot}}(\mathrm{H}_2) - n\Delta E_{\mathrm{sol}}, \tag{2}$$

where $E_{\mathrm{tot,gb/s}}^{\mathrm{GB}}(38\mathrm{Fe}, n\mathrm{H})$ is the total energy for the most stable state with n hydrogen atoms over the unit-cell area of A ($= 0.278\,\mathrm{nm}^2$) along the GB or FS, and $E_{\mathrm{tot}}^{\mathrm{GB}}(38\mathrm{Fe})$ is the total energy of the clean Fe GB system. For the calculations of $E_{\mathrm{tot,gb/s}}^{\mathrm{GB}}(38\mathrm{Fe}, n\mathrm{H})$ and $E_{\mathrm{tot}}^{\mathrm{GB}}(38\mathrm{Fe})$, the cutoff energy of 280 eV and $8 \times 4 \times 1$

Monkhorst–Pack k-point meshes are applied. Only the atomic positions are relaxed (the cell volume and shape are fixed). $E_{\mathrm{tot}}(H_2)$ in Equation (2) is calculated using the same cutoff energy (280 eV) for the consistency of numerical accuracy.

In an effort to calculate the variation of the segregation energy of hydrogen with coverage, hydrogen atoms are progressively added in the following way. First, a single hydrogen atom ($n=1$) is placed at all possible interstitial sites in the cell, and energetically favorable segregation sites are identified. Second, the number of segregated hydrogen atoms is increased ($n \geq 2$) in the same cell, and the most favorable segregation configuration associated with the lowest total energy is individually identified for each number of hydrogen atoms along the GB or the FS within the unit-cell area of A.

For the convenience of later estimating the segregation coverage, the incremental segregation energy is calculated. Considering the maximum number of the segregated sites ($N_{\mathrm{gb/s}}$) over the unit-cell area of A along the GB or the FS, the segregation coverage ($\Gamma_{\mathrm{gb/s}}$) can be defined as

$$\Gamma_{\mathrm{gb/s}} = \frac{n}{N_{\mathrm{gb/s}}}. \tag{3}$$

Alternatively, the segregation energy indicated in Equation (2) is described as a function of the segregation coverage in Equation (4), which is used for the estimation of the cohesive energy later:

$$\Delta E^{\mathrm{seg}}_{\mathrm{gb/s}}(\Gamma_{\mathrm{gb/s}}) = \Delta E^{\mathrm{seg}}_{\mathrm{gb/s}}(n)\Big|_{n=\Gamma_{\mathrm{gb/s}}N_{\mathrm{gb/s}}}. \tag{4}$$

The incremental segregation energy for a single hydrogen atom ($\Delta E^{\mathrm{seg,inc}}_{\mathrm{gb/s}}$) can be determined by the derivative of $\Delta E^{\mathrm{seg}}_{\mathrm{gb/s}}$ with respect to n, and tends to incline down to lower negative values as one more hydrogen atom is added in Equation (5),

$$\Delta E^{\mathrm{seg,inc}}_{\mathrm{gb/s}}(\Gamma_{\mathrm{gb/s}}) = \frac{\partial \Delta E^{\mathrm{seg}}_{\mathrm{gb/s}}(n)}{\partial n}\bigg|_{n=\Gamma_{\mathrm{gb/s}}N_{\mathrm{gb/s}}} = \frac{\partial \Delta E^{\mathrm{seg}}_{\mathrm{gb/s}}(\Gamma_{\mathrm{gb/s}})}{\partial \Gamma_{\mathrm{gb/s}}}\frac{1}{N_{\mathrm{gb/s}}}. \tag{5}$$

2.3. *Generalization of McLean's formula for interacting solute segregation along the grain boundary and fracture surface*

McLean [18] has formulated an equilibrium segregation law on the assumption that segregated solute atoms do not interact with each other. In this case, a change of the total free energy induced by solute segregation (ΔF) is represented by a constant segregation energy per solute atom ($\Delta e^{\mathrm{seg}}_{\mathrm{gb/s}}$), independent of the segregation coverage, together with the number of segregated solute atoms and segregation sites along the GB/FS ($p_{\mathrm{gb/s}}$ and $P_{\mathrm{gb/s}}$) and that of solute atoms and sites in the bulk (p_{b} and P_{b}),

$$\Delta F = \Delta e^{\mathrm{seg}}_{\mathrm{gb/s}}\, p_{\mathrm{gb/s}} - k_{\mathrm{B}}T \ln\left(\frac{P_{\mathrm{gb/s}}!}{p_{\mathrm{gb/s}}!(P_{\mathrm{gb/s}}-p_{\mathrm{gb/s}})!}\frac{P_{\mathrm{b}}!}{p_{\mathrm{b}}!(P_{\mathrm{b}}-p_{\mathrm{b}})!}\right), \tag{6}$$

where k_{B} is Boltzmann's constant and T is the absolute temperature. The occupation of hydrogen in the bulk lattice and the segregation coverage along GB/FS (Γ_{b} and $\Gamma_{\mathrm{gb/s}}$) are given by $p_{\mathrm{b}}/P_{\mathrm{b}}$ and $p_{\mathrm{gb/s}}/P_{\mathrm{gb/s}}$, respectively. Assuming a single hydrogen atom occupies an interstitial tetrahedral site, the hydrogen content in the bulk lattice

of bcc Fe (C_H) is given by

$$C_H = \frac{p_b}{P_b/6 + p_b} \approx \frac{6p_b}{P_b} = 6\Gamma_b \tag{7}$$

in units of atomic fraction, where the number of Fe atoms is $P_b/6$ and $P_b \gg p_b$. The vibrational entropy term is neglected for the sake of simplicity.

Considering that the segregation energy of solute atoms in the system changes depending on the number of segregated solute atoms for both the GB and FS, Equation (6) can be generalized by replacing $\Delta e^{seg}_{gb/s} p_{gb/s}$ with a general function of $\Delta\varepsilon^{seg}_{gb/s}(p_{gb/s})$. This method is more general than Hondros and Seah's extension of McLean's formula [23]; the solute interaction energy is restricted to be proportional to the solute concentration. By minimizing ΔF under the condition of $p_{gb/s} + p_b = \text{const.}$, the generalized McLean's formula for the interacting solute system is obtained as

$$\frac{\Gamma_{gb/s}}{1-\Gamma_{gb/s}} = \frac{\Gamma_b}{1-\Gamma_b}\exp\left(\frac{-\Delta\varepsilon^{seg,inc}_{gb/s}(\Gamma_{gb/s})}{k_B T}\right), \tag{8}$$

$$\Delta\varepsilon^{seg,inc}_{gb/s}(\Gamma_{gb/s}) = \left.\frac{\partial\Delta\varepsilon^{seg}_{gb/s}(p_{gb/s})}{\partial p_{gb/s}}\right|_{p_{gb/s}=\Gamma_{gb/s}P_{gb/s}}. \tag{9}$$

In this derivation, Stirling's approximation ($\ln N! \approx N\ln N - N$) is used. It is equivalent to a derivation from the condition that the chemical potentials of hydrogen remain the same in the GB/FS and bulk. In iron with low-yield strength, the effect of hydrostatic stresses acting upon the GB can be ignored and the chemical potentials of the GB/FS ($\mu_{gb/s}$) and bulk (μ_b) are given as

$$\mu_{gb/s}(\Gamma_{gb/s}) = \left.\frac{\partial\Delta F}{\partial p_{gb/s}}\right|_{p_{gb/s}=\Gamma_{gb/s}P_{gb/s}} = \Delta\varepsilon^{seg,inc}_{gb/s}(\Gamma_{gb/s}) + k_B T\ln\frac{\Gamma_{gb/s}}{1-\Gamma_{gb/s}}, \tag{10}$$

$$\mu_b(\Gamma_b) = \left.\frac{\partial\Delta F}{\partial p_b}\right|_{p_b=\Gamma_b P_b} = k_B T\ln\frac{\Gamma_b}{1-\Gamma_b}. \tag{11}$$

The incremental segregation energy ($\Delta\varepsilon^{seg,inc}_{gb/s}$) is defined as the energy change by adding one solute atom at a segregation site when the number of segregated solute atom is $p_{gb/s}(= \Gamma_{gb/s}P_{gb/s})$. Later the incremental segregation energy of the general form ($\Delta\varepsilon^{seg,inc}_{gb/s}$) in Equation (8) is replaced with $\Delta E^{seg,inc}_{gb/s}$ which is calculated from first principles. Consequently, the generalized McLean's equation will be numerically solved by self-consistent iterations.

2.4. *Intergranular cohesive energies under the conditions of constant composition and chemical potential*

Two types of intergranular decohesion under the conditions of constant composition and chemical potential are controlled by a reduction of the GB and FS segregation

Table 1. Calculated grain-boundary energy (γ_{gb}) of bcc Fe Σ3(111) GB, (111) fracture surface energy (γ_s), together with solid solution energy of hydrogen in bcc Fe.

	γ_{gb} (J/m^2)	γ_s (J/m^2)	ΔE_{sol} (t site) (eV/atom)
Calc.	1.52	2.69	0.21
Exp. [24]	–	–	0.30

energy, which is affected by the quantity of segregated hydrogen (Figure 1). Note that the hydrogen mobility and GB cracking rate interplay. The relationships of the GB/FS segregation energies ($\Delta E^{seg}_{gb/s}$) to the hydrogen coverage are established by using first-principles calculations. Then the GB/FS coverage is correlated with Γ_b by the generalized McLean's formula (Equation 8), together with the incremental GB/FS segregation energies of hydrogen ($\Delta E^{seg,inc}_{gb/s}$).

Intergranular cohesive energy is differently affected by the conditions of constant composition and chemical potential linked with the hydrogen mobility. Immobile hydrogen atoms exert intergranular embrittlement, thus causing fast crack growth (Figure 1a). The same number of hydrogen atoms can be maintained along the GB before fracture and on the two FSs after fracture within the unit-cell area; therefore, each hydrogen coverage (Γ_i) on the two FSs is given by $\Gamma_{gb}N_{gb}/(2N_s)$. Under the mobile hydrogen condition, possibly constant chemical potential (Figure 1b), slow crack propagation allows hydrogen to diffuse from the bulk and/or GB on its two FSs, so that the hydrogen coverage on the two FSs can be magnified independent of the GB coverage. Consequently, the intergranular cohesive energy caused by mobile as well as immobile hydrogen is related to different FS coverages,

$$2\gamma_{int}(\Gamma_b) = 2\gamma_s + 2\Delta E^{seg}_s(\Gamma_i)/A - \left\{\gamma_{gb} + \Delta E^{seg}_{gb}(\Gamma_{gb})/A\right\}, \quad (12)$$

where $\Gamma_i = \Gamma_{gb}N_{gb}/(2N_s)$ for the constant composition and $\Gamma_i = \Gamma_s$ for the constant chemical potential. In Equation (12), γ_s and γ_{gb} are the fracture surface and grain boundary energies, respectively, without hydrogen segregation (Table 1). It is pointed out that the relationships between $\Gamma_{gb/s}$ and Γ_b can be numerically determined from the self-consistent solutions of the generalized McLean's formula (Equation 8) with the incremental segregation energy calculated from first-principles. Equation (12) is a simplified form of the original one by Hirth and Rice [10], consisting of only internal energy terms.

3. Results

3.1. *Grain-boundary energy, surface energy and solid–solution energy of hydrogen*

The calculated energies of pure bcc Fe Σ3(111) GB and (111) FS are shown in Table 1. From these data, $2\gamma_{int}$ of the pure GB is 3.86 J/m^2. The solid–solution energy of hydrogen in bcc Fe is also shown in this table. The solid–solution state of hydrogen at the t site (0.21 eV/atom) is a little more stable than that at the o site (0.35 eV/atom). This is consistent with Christmann's result [24]. The positive

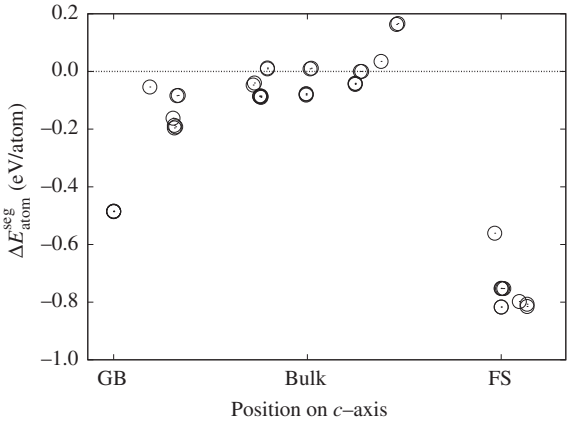

Figure 3. Segregation energy of a single hydrogen atom at all possible interstitial sites in the unit cell ($\Delta E^{seg}_{atom} = \Delta E^{seg}_{gb/s}$; $n = 1$), which is calculated relative to the solid solution energy at a tetrahedral site. Negative energy means stable energetically. The largest segregation energies (negative) are −0.48 eV/atom for the GB, and −0.82 eV/atom for the fracture surface (FS).

solid–solution energy indicates that hydrogen cannot easily dissolve in the bcc Fe lattice. Although our calculations do not include the zero-point energy of hydrogen, the calculated solid–solution energy is in rough agreement with the experimental observations (Table 1) [24].

3.2. *Hydrogen segregation energy for low coverage*

The calculated segregation energy ($\Delta E^{seg}_{atom} = \Delta E^{seg}_{gb/s}$; $n = 1$) is shown in Figure 3 for the placement of a single hydrogen atom at all possible segregation sites in the unit cell. From this figure, it is indicated that the largest segregation energy (negative) at the GB is −0.48 eV/atom, whereas that on the FS is −0.82 eV/atom. This indicates that hydrogen more preferentially segregates on the FS than along the GB.

A wide variety of intergranular segregation energy of hydrogen in iron alloys has been experimentally observed to be −0.1 [25], −0.51 [26], and −0.61 [27] eV/atom. Such diversity is likely related to the structure dependence, the hydrogen detectability of various experimental techniques, and the coverage dependence. The (111) surface segregation energy was estimated to be −0.75 eV/atom [24] from the experimental data of adsorption energy on the (111) surface and solid–solution energy, which is in crude agreement with the calculated result. The discrepancy may be due to the zero-point energy, which is not included in our calculations.

3.3. *Relationships between hydrogen segregation energy and coverage*

The first-principles calculations indicate how $\Delta E^{seg}_{gb/s}$ and $\Delta E^{seg,inc}_{gb/s}$ change with the number of segregated hydrogen atoms along the GB and on its (111) FS (Figure 4) within the unit-cell area of A (0.278 nm^2). In these calculations, the energetically most stable configuration of hydrogen segregation was determined for each number

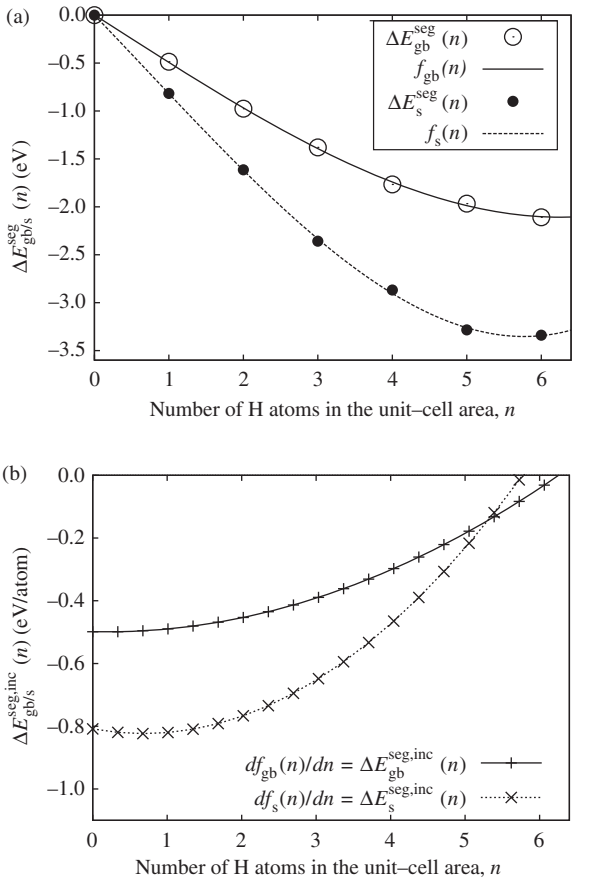

Figure 4. (a) Variation of calculated segregation energy of the energetically most stable segregation configuration ($\Delta E^{seg}_{gb/s}(n)$) with increasing number of hydrogen atoms (n) along the GB/FS in the unit-cell area of A (0.278 nm^2). $f_{gb/s}(n)$ indicates a third-order polynomial function for fitting. (b) The incremental segregation energy of one hydrogen atom ($\Delta E^{seg,inc}_{gb/s}(n)$), given by the derivative of $f_{gb/s}(n)$ with respect to n, is plotted against the number of segregated hydrogen atoms (n).

of segregated hydrogen atoms. An important finding is that $\Delta E^{seg,inc}_{gb/s}$ reaches zero at about six hydrogen atoms, $N_{gb} = 6.257$ and $N_s = 5.772$, over the unit-cell area of A along the GB and on the FS, respectively. This corresponds to the full segregation coverage. The variation of the calculated $\Delta E^{seg}_{gb/s}$ with n can be fitted with a third-order polynomial function of n in Figure 4a. The incremental segregation energy is given by a second-order function, according to Equation (5). Then, the relationships of ΔE^{seg}_{gb} and $\Delta E^{seg,inc}_{gb}$ to Γ_{gb} are described by

$$\Delta E^{seg}_{gb}(\Gamma_{gb}) = 0.003 - 3.12\,\Gamma_{gb} - 0.094\,\Gamma^2_{gb} + 1.102\,\Gamma^3_{gb}, \tag{13}$$

$$\Delta E^{seg,inc}_{gb}(\Gamma_{gb}) = -0.499 - 0.030\,\Gamma_{gb} + 0.529\,\Gamma^2_{gb}, \tag{14}$$

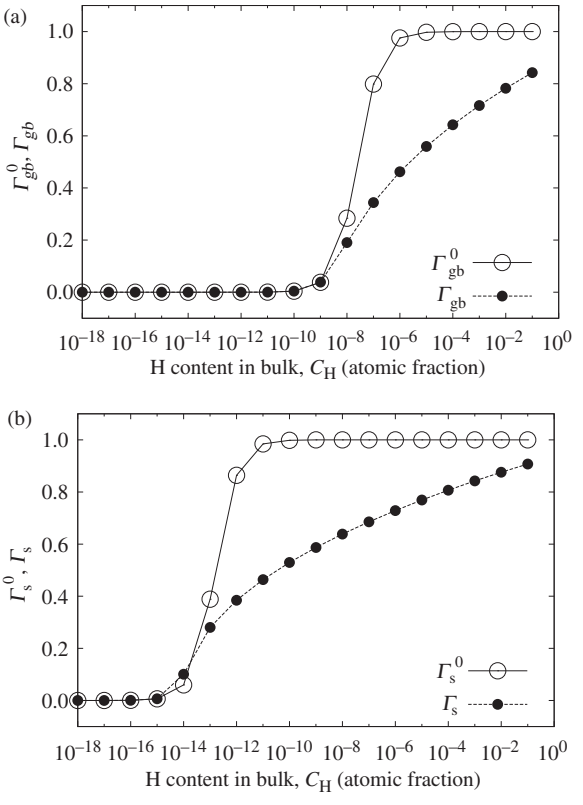

Figure 5. Comparison of the variation of hydrogen coverage along the GB (a) and FS (b) at the temperature of 300 K. $\Gamma^0_{gb/s}$ is the coverage value calculated from the original McLean's formula for a non-interacting solute system with constant segregation energy (−0.48 eV/atom for GB, −0.82 eV/atom for FS). $\Gamma_{gb/s}$ is the coverage value calculated from the generalized McLean's formula (Equation 8) for an interacting solute system with incremental segregation energy ($\Delta E^{seg,inc}_{gb/s}$) as shown in Figure 6.

in units of eV and eV/atom, respectively. Similarly, the two segregation energies for the FS are given as a function of Γ_s (= n/N_s) by

$$\Delta E^{seg}_s(\Gamma_s) = 0.001 - 4.667\,\Gamma_s - 0.728\,\Gamma_s^2 + 2.041\,\Gamma_s^3, \tag{15}$$

$$\Delta E^{seg,inc}_s(\Gamma_s) = -0.808 - 0.252\,\Gamma_s + 1.061\,\Gamma_s^2. \tag{16}$$

By substituting $\Delta E^{seg,inc}_{gb/s}$ in the generalized McLean's formula (Equation 8), these equations were numerically solved by self-consistent iterations to obtain the GB/FS coverage at the temperatures of 300 K and 170 K, and over a wide range of C_H ($6\Gamma_b$). As shown in Figure 5, it can be seen that the hydrogen segregation coverage ($\Gamma_{gb/s}$) along the GB/FS increase more gradually with increasing C_H, compared with that not associated with the interaction of segregated hydrogen ($\Gamma^0_{gb/s}$). Such behavior is physically reasonable, because the enhancement of the repulsive interactions among

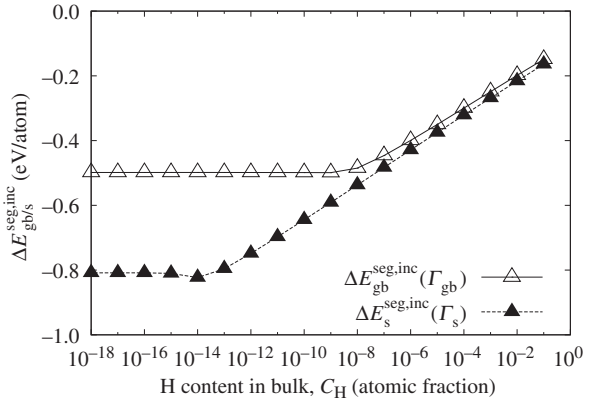

Figure 6. Variation of the incremental segregation energies ($\Delta E_{gb/s}^{seg,inc}$) for GB and FS with increasing bulk hydrogen content (C_H). These energies are determined from the generalized McLean's formula in Equation (8) by numerical self-consistent iterations at the temperature of 300 K.

segregated hydrogen atoms reduces the incremental segregation energy (Figure 6) and suppresses the increase of coverage.

3.4. *Reduction of GB cohesive energy*

As mentioned earlier, the effect of C_H ($6\Gamma_b$) on changing intergranular cohesive energy induced by the mobile and/or immobile effects of hydrogen can be investigated by using the generalized McLean's formula (Equation 8) and the cohesive energy formula (Equation 12), together with the segregation energies (Equations 13–16). The calculated chemical potentials using Equations (10) and (11) for GB/FSs are plotted against the coverage in Figure 7. In this diagram, the two types of fast and slow GB fracture are highlighted under the conditions of constant composition and chemical potential, respectively.

The results for intergranular decohesion by a sole immobile effect and combined mobile and immobile effects of hydrogen segregation are illustrated in Figure 8. Interestingly, the combined mobile and immobile effects of hydrogen cause easy occurrence of intergranular decohesion at a very lower C_H value of 10^{-14} (10^{-24}) atomic fraction at the temperature of 300 K (170 K), in comparison with immobile hydrogen-induced decohesion over more than C_H of 10^{-9} (10^{-16}) atomic fraction. The reason for the strong decohesion effect of mobile hydrogen is that the segregation energy of hydrogen on the FS (−0.82 eV/atom) is much larger (negative) than that at the grain boundary (−0.48 eV/atom) under ambient temperatures. It is noted that the decohesion induced by the combined mobile and immobile hydrogen is slightly weakened by further increasing the bulk hydrogen content due to the decreased grain boundary energy. As the mobile effect of hydrogen becomes effective, it is reasonable that more hydrogen atoms can be adsorbed on the two FSs as a result of a sufficient supply of diffusive hydrogen atoms, and the stronger

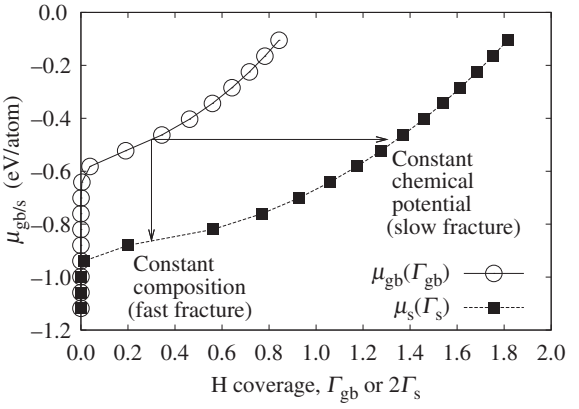

Figure 7. Calculated chemical potentials along GB/FS (μ_{gb}/μ_s) as a function of coverage ($\Gamma_{gb/s}$) at 300 K. $\mu_s(\Gamma_s)$ is plotted with increasing $2\Gamma_s$, because hydrogen atoms segregate along two fracture surfaces (FSs). The number of hydrogen atoms segregated along GB/FSs on the area of $A/2A$ (A=0.278 nm^2) can be obtained as $\Gamma_{gb}N_{gb}/2\Gamma_sN_s$ ($N_{gb} = 6.257/N_s = 5.772$). The two types of concepts of fracture under the conditions of constant composition (fast fracture) and chemical potential (slow fracture) are indicated by vertical and horizontal arrows, respectively.

intergranular decohesion would be achieved. The self-consistent solutions indicate that the incremental segregation energy of hydrogen on the FS is much larger (negative) than that along the GB over a wide range of C_H (Figure 6).

4. Discussion

4.1. *Estimation of diffusion time*

The trajectory of composition vs. chemical potential shown in the diagram for GB and FS delineates two distinct features of intergranular fast and slow fracture, respectively, under the conditions of constant composition and chemical potential (Figure 7). The mobile hydrogen during slow decohesion causes more remarkable GB embrittlement, compared with the immobile one. It is necessary to evaluate how quickly hydrogen diffuses to the GB and FS for achieving the condition of constant composition and chemical potential. As schematically indicated in Figure 9, three diffusion paths of hydrogen – (i) from the bulk to the GB, (ii) from the bulk to the FS, and (iii) from the GB to the two FSs – are considered. In this figure, the hydrogen diffusion to the FS is regarded towards the near-tip zone of a slowly growing crack. Based on McLean's kinetic theory [18], the diffusion time (t_d) of hydrogen segregation into the GB and FS necessary for half equilibrium is affected by the enrichment factor (α), which is represented by the ratio of hydrogen content at the segregation sites to that at the diffusion source, as well as the hydrogen diffusivity in the bulk and along the GB (D; D_b and D_{gb}),

$$t_d = 9\alpha^2 d^2/(16FD). \tag{17}$$

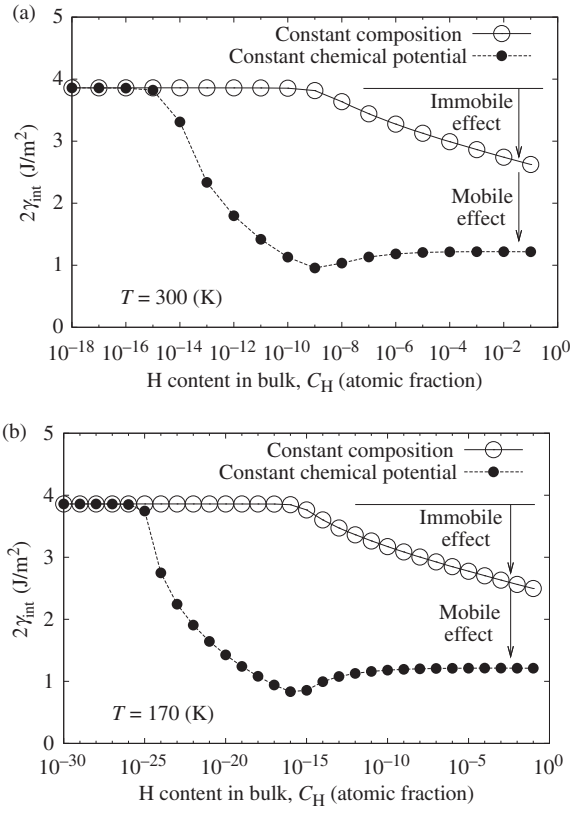

Figure 8. Comparison of the reduction of cohesive energy ($2\gamma_{int}$) of bcc Fe Σ3(111) GB, caused by only the immobile effect of hydrogen under the condition of constant composition (fast fracture), and both of the mobile and immobile effects of hydrogen under the condition of constant chemical potential (slow fracture), with increasing bulk hydrogen content (C_H) at (a) 300 K and (b) 170 K.

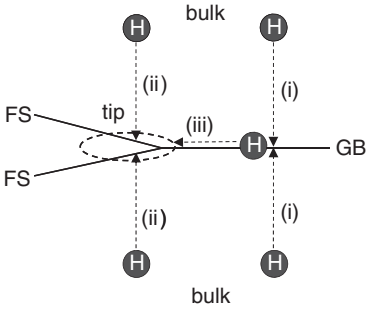

Figure 9. Schematic illustration of three diffusion paths (i)–(iii) for hydrogen.

In Equation (17), the thickness of the segregation region (d) is set as the interlayer distance of (111) plane in bcc Fe ($d_{(111)} = 0.0818$ nm) and F is a configuration factor depending on the segregation region (4 for the GB and 1 for the FS) [28]. The hydrogen diffusivity along the GB can be estimated with the incremental segregation energy that changes with hydrogen coverage (Equation 14). The parameter settings for the three diffusion paths are described in Appendix B.

The diffusion time of hydrogen strongly depends on the path and the bulk hydrogen content, and is influenced by the enrichment factor (Figure 10a). The diffusion path (i) from the bulk to the GB allows hydrogen to reach half equilibrium more rapidly, compared with (ii) from the bulk to the FS in the whole range of C_H. This is due to the smaller enrichment factor and the larger configuration factor of the path (i). Hydrogen diffusion from the GB to the two FSs (iii) brings about the shortest time-lag for C_H above 10^{-11} atomic fraction, although the GB diffusion of hydrogen is slowed down by the trapping effect. In path (iii), the enrichment factor reduced by the high GB coverage overwhelms the sluggish effect of hydrogen diffusion. Thus, it can be reasoned that hydrogen would reach FS segregation sites newly generated by slow separation of the GB not directly from the bulk but though the GB.

A comparison of the variations of diffusion time necessary for the slow and fast fracture and GB cohesive energy with C_H at the temperature of 300 K is shown in Figure 10b. It can be seen that regardless of whether intergranular cracking occurs slowly or rapidly, the incubation time for the half hydrogen accumulation is the same except for $C_H < 10^{-11}$ atomic fraction. The onset of decreasing the diffusion time of hydrogen for both the (i), and (i) plus (iii) paths coincides with that of the initiating fast decohesion and the maximum slow decohesion, which are controlled by the sole immobile hydrogen and combined mobile and immobile hydrogen, respectively, under the conditions of constant composition and chemical potential. Therefore, it is difficult to judge how mobile or immobile segregated hydrogen, or both play a dominant role on the GB decohesion in terms of the time delay.

4.2. *Comparison with experimental observations*

In an effort to distinguish the fast and slow cracking behavior, it is imperative to conduct experiments on notched or precracked specimens with large grain sizes comparable to the specimen thickness or bamboo type grains, and/or monitoring acoustic emissions [29]. Smooth tensile specimens of high-purity iron with coarse and bamboo grains were tested at about 170 K under the dynamical and precharging of hydrogen with the current density of 20 and more than 100 A/m^2, respectively [30,31]. Comparing this with the dynamic charging of 20 A/m^2 resulting in more than 10^{-6} atomic fraction [32], the larger current-density precharging would not necessarily produce a higher bulk hydrogen content due to the easy release of hydrogen from the high-purity bamboo-structured iron with its weak hydrogen trapping [33]. The tensile specimens dynamically and precharged with hydrogen exhibited a sudden and gradual drop in the applied stress, indicative of the GB fast and slow cracking, respectively. The short initiation time of about 160 and 60 seconds identified for the fast and slow cracking are consistent with the diffusion time of hydrogen at 170 K along the paths (i), and (i) plus (iii) estimated for the two

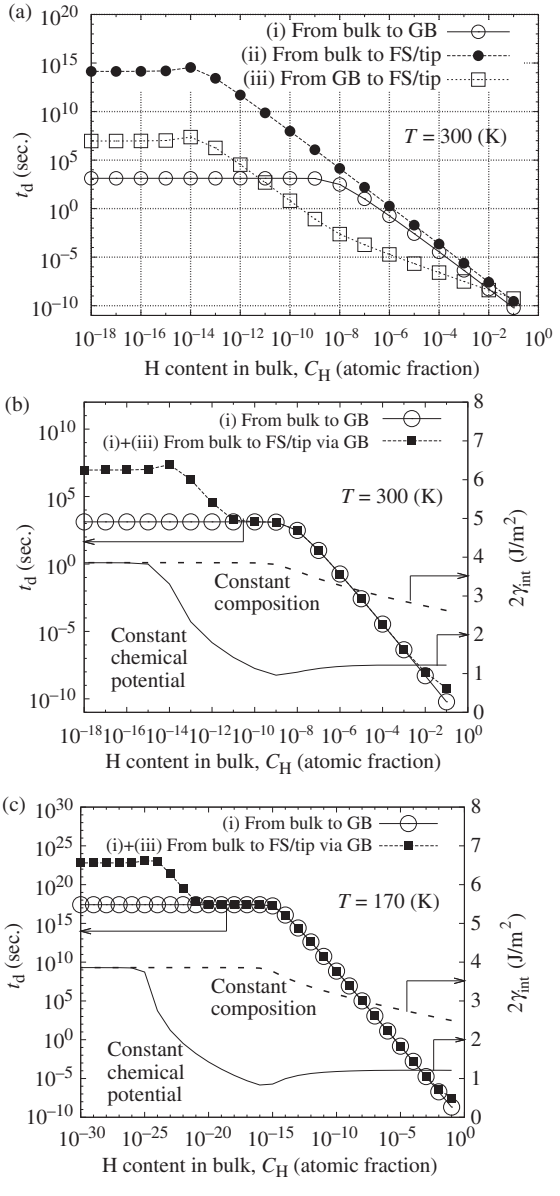

Figure 10. (a) Simple estimation of the diffusion time (t_d) of hydrogen segregation required for achieving the half equilibrium state at the temperature of 300 K. The three diffusion paths (i)–(iii) are illustrated in Figure 9. Comparison of the variations of diffusion time for fast (constant composition) and slow (constant chemical potential) fracture and GB cohesive energy at (b) 300 K and (c) 170 K.

types of cracking for C_H of about 10^{-6} atomic fraction (Figure 10c). Nonetheless, both slow and fast cracking occurred near yielding as controlled by microcrack nucleation in the smooth tensile specimens (Appendix A), despite the different magnitudes in the two types of GB decohesion (Figure 8b).

Furthermore, iron containing C contents of more than 20 mass ppm showed ductile fracture even under more severe dynamical hydrogen-charging conditions [30]. The mitigating effect of C addition on hydrogen-induced GB cracking is supported by the previous first-principles calculations indicating the GB strengthening effect of segregated C [16]. In ultra-high-strength steels with C_H more than 10^{-7} atomic fraction in the triaxially stressed lattice [34], moreover, it is speculated that easy occurrence of intergranular slow cracking would be responsible for lowering the threshold stress intensity factor. For the purpose of clarifying intergranular hydrogen embrittlement mechanisms of ultra-high-strength steel, a detailed first-principles study is now in progress in the light of the competitive segregation of hydrogen, manganese (Mn) and/or C on the GB and FS, thereby exerting the embrittling and strengthening effects [35–37].

5. Conclusions

The decohesion behavior caused by mobile as well as immobile hydrogen effects along a bcc Fe $\Sigma3(111)$ symmetrical tilt grain boundary (GB) has been analyzed by first-principles calculations. The variations of two types of hydrogen segregation energy over a unit-cell area and its derivative (incremental) with respect to the number of hydrogen atoms along the GB and its (111) FS were determined as polynomial functions of the hydrogen coverage. This is physically reasonable segregation behavior: the hydrogen segregation diminishes down to zero near the full coverage by maximizing the repulsive interactions of segregated hydrogen atoms. By generalizing McLean's segregation theory where the segregation energy and coverage are incorporated with each other under specified temperatures and bulk hydrogen concentrations, the segregation energy and coverage are numerically determined for various bulk hydrogen contents by self-consistent iterations.

The intergranular cohesive energy of iron, represented by a change in the hydrogen segregation energy and coverage along the GB and FS, was calculated over a wide range of bulk hydrogen at the temperatures of 300 K and 170 K. It has been investigated whether the mobile or immobile effects of hydrogen or both strongly influence the intergranular decohesion. The present calculated results for the iron–hydrogen system indicate that a very low bulk content of hydrogen (about 10^{-9} atomic fraction) is necessary for achieving the maximum intergranular decohesion induced by mobile hydrogen under the condition of constant chemical potential at 300 K. The cohesive energy of the GB is largely (70–80%) reduced by the combined mobile and immobile effects of hydrogen, whereas it is only 10–20% decreased by the sole immobile effect. This is ascribed to a larger segregation energy (negative) of hydrogen on the FS than that at the GB. As a first approximation, the diffusion time of hydrogen from the GB onto the FSs is reasonably shorter than from the bulk, thereby causing mobile hydrogen-induced GB decohesion.

Acknowledgments

We thank E. Akiyama, Y. Kimura, K. Tsuzaki, and T. Suzudo for helpful discussions. The calculations were performed on the supercomputer Fujitsu BX900 system in Japan Atomic Energy Agency (JAEA). This study was carried out as a part of research activities of ''Fundamental Studies on Technologies for Steel Materials with Enhanced Strength and Functions'' by Consortium of JRCM (The Japan Research and Development Center of Metals). Financial support from NEDO (New Energy and Industrial Technology Development Organization) is gratefully acknowledged.

References

[1] J.P. Hirth, Metall. Trans. A 11 (1980) p.861.
[2] B. Somerday, P. Sofronis and R. Jones (eds.), *Effects of Hydrogen on Materials: Proceedings of the 2008 International Hydrogen Conference*, September 7–10, 2008, Jackson Lake Lodge, Grand Teton National Park, Wyoming, USA, 2008.
[3] R.P. Gangloff, *6.02 – Hydrogen-assisted cracking*, in *Comprehensive Structural Integrity*, I. Milne, R.O. Ritchie and B. Karihaloo, eds., Pergamon Press, Oxford, 2003, p.31.
[4] N.J. Petch and P. Stables, Nature 169 (1952) p.842.
[5] A. Troiano, Trans. ASM 52 (1960) p.54.
[6] R.A. Oriani, *Stress corrosion cracking and hydrogen embrittlement of iron base alloys*, in *International Corrosion Conference Series*; NACE-5, 1977, p.351.
[7] C.D. Beachem, Metall. Trans. 3 (1972) p.437.
[8] H. Birnbaum and P. Sofronis, Mater. Sci. Eng. A 176 (1994) p.191.
[9] J.R. Rice, *Hydrogen and interfacial cohesion*, in *Effect of Hydrogen on Behavior of Materials*, A.W. Thompson and I.M. Bernstein, eds., Metallurgical Society of AIME, New York, 1976, p.455.
[10] J.P. Hirth and J.R. Rice, Metall. Trans. A 11 (1980) p.1501.
[11] J.R. Rice and J.-S. Wang, Mater. Sci. Eng. A 107 (1989) p.23.
[12] J. Kameda, Acta Metall. 34 (1986) p.867.
[13] L. Zhong, R. Wu, A.J. Freeman and G.B. Olson, Phys. Rev. B 62 (2000) p.13938.
[14] W.-T. Geng, A.J. Freeman, G.B. Olson, Y. Tateyama and T. Ohno, Mater. Trans., JIM 46 (2005) p.756.
[15] Z.X. Tian, W. Yan, J.X. Hao and W. Xiao, J. Phys.: Cond. Matt. 23 (2011), Article No. 015501.
[16] M. Yamaguchi, Metall. Mater. Trans. A 42 (2011) p.319.
[17] M. Yamaguchi, K.-I. Ebihara, M. Itakura, T. Kadoyoshi, T. Suzudo and H. Kaburaki, Metall. Mater. Trans. A 42 (2011) p.330.
[18] D. McLean, *Grain Boundaries in Metals*, Oxford University Press, Oxford, 1957.
[19] G. Kresse and J. Hafner, Phys. Rev. B 47 (1993) p.R558.
[20] G. Kresse and J. Furthmüller, Phys. Rev. B 54 (1996) p.11169.
[21] G. Kresse and D. Joubert, Phys. Rev. B 59 (1999) p.1758.
[22] J.P. Perdew, K. Burke and M.P. Ernzerhof, Phys. Rev. Lett. 77 (1996) p.3865.
[23] E.D. Hondros and M.P. Seah, Metall. Mater. Trans. A 8 (1977) p.1363.
[24] K. Christmann, Surf. Sci. Rep. 9 (1988) p.1.
[25] W. Choo and J. Lee, Metall. Trans. A 13A (1982) p.135.
[26] K. Ono and M. Meshii, Acta Metall. Mater. 6 (1992) p.1357.
[27] T. Asaoka, C. Dagbert, M. Aucouturier and J. Galland, Scripta Metall. 11 (1977) p.467.
[28] M.P. Seah, *AES in metallurgy*, in *Practical Surface Analysis*, 2nd ed., D. Briggs and M.P. Seah, eds., John Wiley, New York, 1990, p.311.
[29] J. Kameda, Acta Metall. 34 (1986) p.1721.

[30] A. Kimura and H. Kimura, J. Japan Inst. Metals 47 (1983) p.807 (in Japanese).
[31] S. Moriya, H. Matsui and H. Kimura, Mater. Sci. Eng. 40 (1979) p.217.
[32] A. Kimura, Personal communication, Kyoto University, 2011.
[33] S. Moriya, S. Takaki and H. Kimura, Mater. Sci. Eng. 32 (1978) p.71.
[34] N. Bandyopadhyay, J. Kameda and C.J. McMahon Jr, Metall. Trans. A. 14 (1983) p.881.
[35] D.Y. Lee, E.V. Barrera, J.P. Stark and H.L. Marcus, Metal. Trans. A 15 (1984) p.1415.
[36] Y.Q. Weng and C.J. McMahon Jr, Mater. Sci. Technol. 3 (1987) p.207.
[37] S. Suzuki, M. Obata, K. Abiko and H. Kimura, Trans. ISIJ 25 (1985) p.62.
[38] A.A. Griffith, Phil. Trans. R. Soc. Lond. A 221 (1921) p.163.
[39] E. Orowan, Rep. Prog. Phys. 12 (1949) p.185.
[40] G.R. Irwin, J. App. Mech. 24 (1957) p.361.
[41] M.L. Jokl, V. Vitek and C.J. McMahon Jr, Acta Metall. 28 (1980) p.1479.
[42] J. Kameda and C.J. McMahon Jr, Metal. Trans. 11A (1980) p.91.

Appendix A. GB cracking mechanism

The microscopic mechanism of hydrogen-induced GB cracking is illustrated in iron. The intergranular cohesive energy and plastic work ($2\gamma_{\text{int}}$ and γ_p) are fundamental physical properties manifesting the extent of hydrogen embrittlement. Hydrogen-induced GB cracking is controlled by the nucleation and growth of microcracks. Oxides lying along the GB, even in high-purity iron [30,31], serve as nuclei under localized plasticity due to the pileup of dislocations.

The energy balance criterion governs the growth of a nucleated microcrack along the GB [38–40]. The strain energy release rate expressed by the critical driving stress (σ^*) depending on the type of specimens used, the half microcrack size (a_c) and Young's modulus (E) and Poisson's ratio (ν) is required to exceed $2\gamma_{\text{int}}$ plus γ_p.

$$(1-\nu^2)\,\pi\,(\sigma^*)^2 a_c/E \geq 2\gamma_{\text{int}} + \gamma_p. \tag{A1}$$

The segregation of mobile as well as immobile hydrogen along the GB and microcrack surface differently controls the reduction in $2\gamma_{\text{int}}$. Although γ_p expended for the dislocation activities near the tip of a growing microcrack is one order of magnitude larger than $2\gamma_{\text{int}}$, γ_p changes exponentially dependent on $2\gamma_{\text{int}}$ due to the concomitant processes of GB decohesion and dislocation activities near the microcrack tip [41]. Moreover, hydrogen segregation per se would directly enhance or suppress the nucleation and growth of dislocations. The hydrogen effect on γ_p is beyond the scope of this study. In smooth tensile tests not associated with the localized plasticity, it is pointed out that different magnitudes of GB decohesion could not be clarified, because the microcrack nucleation controls hydrogen-induced GB cracking [42].

Appendix B. Parameters in the analysis of hydrogen diffusion in iron

To analyze the hydrogen segregation required for fast and slow cracking under the conditions of constant composition and chemical potential, the diffusion time (t_{d}) for half equilibrium given by Equation (17) is applied according to McLean's kinetic theory [18]. For calculating t_{d}, three parameters such as the enrichment factor (α), the hydrogen diffusivity in bulk and along the GB (D_{b} and D_{gb}), and the configuration factor (F) are listed in Table B1. The thickness of the segregation region (d) for hydrogen is regarded as the interlayer distance of the (111) plane in the bcc Fe lattice ($d_{(111)} = 0.0818$ nm), because the region was found to be localized within a single atomic layer for both the GB and FS in this study.

Three diffusion paths are considered: (i) from the bulk to the GB; (ii) from the bulk to the FS; and (iii) from the GB to the two FSs. The enrichment factor is set as the ratio among the coverages on GB/FS ($\Gamma_{\text{gb}}/\Gamma_{\text{s}}$) and the occupation in bulk (Γ_{b}), determined by the generalized

Table B1. Parameter settings in Equation (17) for the estimation of the diffusion time of hydrogen for achieving the half equilibrium state. Detailed explanations are given in Appendix B.

	Path	α	F	D
(i)	From bulk to GB	$\Gamma_{gb}/(2\Gamma_b)$	4	D_b
(ii)	From bulk to FS/tip	$\Gamma_s/(2\Gamma_b)$	1	D_b
(iii)	From GB to FS/tip	$2\Gamma_s/\Gamma_{gb}$	1	D_{gb}

McLean's formula in Equation (8) at the temperatures of 300 K and 170 K. As seen in Table B1, the enrichment factor for case (i) and (ii) includes a factor of 1/2 that arises from the difference in the number density of octahedral and tetrahedral sites between the segregation region (GB/FS) and the bulk lattice, respectively. A factor of 2 for case (iii) reflects the two fracture surfaces. According to Seah's analysis [28], F is 4 for diffusion path (i) and 1 for cases (ii) and (iii). The hydrogen diffusivity in bcc Fe at temperate T is estimated from the empirical equation suggested by Hirth [1],

$$D_b = 2.0 \times 10^{-7} \exp(-828/T) \quad (m^2/sec.). \tag{B1}$$

The estimated values are 1.27×10^{-8} and $1.53 \times 10^{-9}\,m^2/sec.$ at $T = 300\,K$ and 170 K, respectively, for cases (i) and (ii). By considering the strong hydrogen trapping at the GB region, the GB hydrogen diffusivity (D_{gb}) is estimated using Boltzmann's factor of the incremental segregation energy at the GB,

$$D_{gb} = D_b \exp\left(\frac{\Delta E_{gb}^{seg,inc}}{k_B T}\right), \tag{B2}$$

where $\Delta E_{gb}^{seg,inc}$ is given as a function of Γ_{gb} in Equation (14).